applied sciences

MDPI

Article

Fully Metallic Additively Manufactured Monopulse Horn Array Antenna in Ka-Band

José Rico-Fernández [1], Álvaro F. Vaquero [2,*], Marcos R. Pino [3] and Manuel Arrebola [3]

[1] Northern Waves AB, 115 43 Stockholm, Sweden; pepe.rico@northern-waves.com
[2] Department of Mathematics, Applied Mathematics, Universidad de Oviedo, 33007 Oviedo, Spain
[3] Group of Signal Theory and Communications, Department of Electrical Engineering, Universidad de Oviedo, 33203 Gijón, Spain; mpino@uniovi.es (M.R.P.); arrebola@uniovi.es (M.A.)
* Correspondence: fernandezvalvaro@uniovi.es

Abstract: The Laser Powder-Bed Fusion Additive Manufacturing (LPBF AM) technique is evaluated for the manufacturing of fully metallic monolithic microwave components. To validate the manufacturing technique, a difference pattern array of 4 × 4 horn antennas is designed to operate at mm-Wave frequencies. The antenna is based on *H*-plane power dividers and a complex structure to obtain a difference radiation pattern by rotating twisted sections in two different orientations. The prototype is manufactured with a monolithic piece of aluminum alloy AlSi10Mg, providing a lightweight single structure that includes both radiating elements and a feeding network consisting of twisters and power dividers in a waveguide. The prototype was experimentally evaluated in an anechoic chamber and the near-field planar acquisition range, obtaining good agreement with full-wave simulations within an operational bandwidth from 34 to 36 GHz. The results demonstrate that the LPBF AM technique is a suitable candidate to produce challenging monolithic metal-only microwave components in the K_a-band, such as monopulse antennas.

Keywords: additive manufacturing; horn array antenna; LPBF; monopulse antenna; difference pattern

check for updates

Citation: Rico-Fernández, J.; Vaquero, Á.F.; Pino, M.R.; Arrebola, M. Fully Metallic Additively Manufactured Monopulse Horn Array Antenna in Ka-Band. *Appl. Sci.* **2024**, *14*, 11065. https://doi.org/10.3390/app142311065

Academic Editor: Hosung Choo

Received: 30 October 2024
Revised: 22 November 2024
Accepted: 24 November 2024
Published: 28 November 2024

Copyright: © 2024 by the authors. Licensee MDPI, Basel, Switzerland. This article is an open access article distributed under the terms and conditions of the Creative Commons Attribution (CC BY) license (https://creativecommons.org/licenses/by/4.0/).

1. Introduction

Additive manufacturing, also known as 3D printing, has had a significant impact on different engineering fields, particularly by presenting a new manufacturing process that enables innovative designs, providing substantial advancements that were not achievable with conventional manufacturing methods. More specifically, AM has had a major impact on the development of antenna concepts in the millimeter-wave (mm-Wave) band. Two key points should be highlighted. First, AM allows the fabrication of intricate designs with complex geometries, achieving relatively high precision, while also enabling novel antenna concepts by utilizing more complex shapes. Secondly, AM enables the rapid prototyping of antennas, not only reducing manufacturing times and costs but also allowing for fast iterations to fine-tune designs, leading to highly optimized solutions. Moreover, AM has opened the door to the use of new materials, ranging from polymers to ceramics and even metals, enabling more cost-effective solutions, as well as designs with reduced volume or weight. Therefore, AM has emerged as an alternative to traditional subtractive manufacturing methods, like Computer Numerical Control (CNC) milling, offering speed, precision, and cost-effectiveness [1]. However, the most important feature that AM provides is the ability to create complex and arbitrary geometries. Thus, it has attracted interest beyond mechanical engineering, notably in antenna engineering.

There are three methodologies that involve manufacturing with AM for antenna and microwave devices. The first method entails the use of dielectric materials for graded-index lenses [2–4], metasurfaces [5], and transmitarrays [6–8]. The second method involves manufacturing dielectric components and subsequently applying metallic coatings, such

as nickel [9,10] or copper [11–14]. Finally, the third method involves metal-only AM techniques, such as AM Laser Powder-Bed Fusion (LPBF), Binder Jetting (BJ), or Directed Energy Deposition (DED), which is ideal for space applications due to its dielectric-loss-free properties and better structural properties. However, AM is not limited solely to radiating elements; it also enables the development of feeding network components, which include various RF devices in waveguide technology, such as filters, twists, or OMTs [1,15,16]. Therefore, AM allows for the development of RF devices that incorporate both the feeding network and radiating elements. To manufacture these designs, a combination of dielectric-material-based fabrication followed by coating can be used to achieve the desired electromagnetic properties. This approach involves dividing the system into multiple parts, ensuring clear access to internal surfaces for coating application. This method presents two potential sources of error. First, it is challenging to guarantee uniform coating throughout the entire structure. Second, the subsequent assembly may introduce minor alignment errors or mismatches, which can cause current leakage and therefore degrade device performance. A second method that eliminates both sources of error is monolithic fabrication. In this approach, access to internal faces is not possible, so metal-based manufacturing (such as LPBF, BF, or DED) is needed. In particular, LPBF AM has been used to develop monolithic microwave components, like waveguide filters [17,18], horn antennas [19], and shaped parallel plate lenses [20–22]. Moreover, the use of monolithic components manufactured by means of this technique has been probed to address and solve alignment issues encountered in milling processes [23], being a suitable technique for designing antenna systems.

Conversely, the role of difference pattern antennas spans various critical applications where precise signal discrimination is essential. In radar systems, they enable the accurate tracking of targets such as aircraft, ships, or weather phenomena by analyzing differences in phase and amplitude among signals received by array elements [24]. Similarly, in wireless communication systems employing beamforming or MIMO techniques, difference pattern antennas improve signal reception and transmission by directing beams toward the desired directions while minimizing interference [25]. In radio astronomy, they facilitate the capture and analysis of celestial signals, assisting astronomers in deciphering the properties of celestial objects through meticulous measurements of signal disparities across the antenna array [26]. Moreover, in direction-finding systems, these antennas are vital for navigation, search and rescue operations, and military endeavors, as they enable the determination of signal source directions by comparing signals received across the array [27]. Difference pattern antennas can be designed using reflective antennas, which integrate four horns as a feed [28]. As an alternative, they have also been designed using either substrate-integrated waveguides (SIWs) [29–31] or metasurfaces [32].

Although SIW-based arrays offer a compact and low-cost solution, their operational bandwidth is limited. Additionally, if electrically large arrays are required, they exhibit high losses in the mm-Wave band due to the necessary substrate. As an alternative, arrays with a corporate feeding network based on waveguide technology and an array of radiating elements, typically slot or horn elements, are often used. By using waveguides in the feeding network, not only is bandwidth increased, but losses are also reduced, as no substrate is required, thereby improving efficiency. Furthermore, this solution is easily scalable. These antennas are typically fabricated by dividing the feeding network into different blocks, each associated with a different RF component (filter, waveguide, OMT, etc.) and radiating elements, using CNC for each of them.

Considering the simplest element, a waveguide section, the manufacturing process is relatively complex in mm-Wave frequencies, as it is usually produced using machined and soldered or brazed techniques, which are not trivial due to the dimensions of the waveguide hole at these frequencies. As the complexity of the feeding network element increases, the fabrication process also becomes more complex. In addition, even when CNC is used, the device must be manufactured in at least two pieces, which requires subsequent assembly with good electrical contact, a non-trivial task. This is where AM, particularly

LPBF, through direct metal printing, can help reduce manufacturing complexities and thus facilitate the design and prototyping of more complex and compact structures.

This work demonstrates the potential of the LPBF AM technique in the design, manufacturing, and experimental validation of critical and precise microwave components in the K_a-band, such as the presented monolithic monopulse antenna with curved surfaces in different directions and small elements in the inner cavities. A difference pattern horn array antenna composed of sixteen elements, which are integrated with 1:4 *H*-plane power dividers and twisted sections in waveguide technology, is manufactured in a fully metallic monolithic piece. The twists are designed in pairs, each with a 180-degree phase difference, which enables counterclockwise phase excitation in the elements, producing a difference pattern. These four twisted components are highly complex to manufacture, as they require curved and rotated surfaces within a relatively small waveguide section. This configuration results in a highly complex yet compact structure that is only feasible through AM, particularly when produced as a single piece. The prototype was manufactured and experimentally validated, demonstrating very stable in-band performance and achieving an operating bandwidth of 10% with almost non-beam squint. These results showcase the potential of LPBF AM in designing antenna systems based on waveguide-fed arrays, allowing for relatively complex and compact designs suitable for monopulse antennas.

2. Difference Pattern Horn Array Antenna Concept

The design of the difference pattern horn array antenna must be conceptualized at the antenna system level, as it will be manufactured monolithically rather than as an integration of independent components. For this purpose, the methodology shown in Figure 1 is followed, where, in the first step, the design is divided into two subsystems: the array of radiating elements and the feeding network. The latter is further subdivided into each of the necessary RF components. Each RF component is designed independently, and once the specifications are met, they are progressively integrated to allow greater control over the feeding network integration. Typically, co-optimization of the RF component chain is performed during this process, requiring only minor dimension adjustments, as the independent designs establish a strong starting point. Once both subsystems are designed, they must be integrated, not only ensuring mechanical assembly but also maintaining RF performance. If any of the established figures of merit are affected by integration, a fine-tuning process is applied to the integrated model until the required specifications are met. Typically, this process requires only minor dimension adjustments; however, if, during integration, the performance deviates significantly from the specifications, the subsystems must be independently redesigned again.

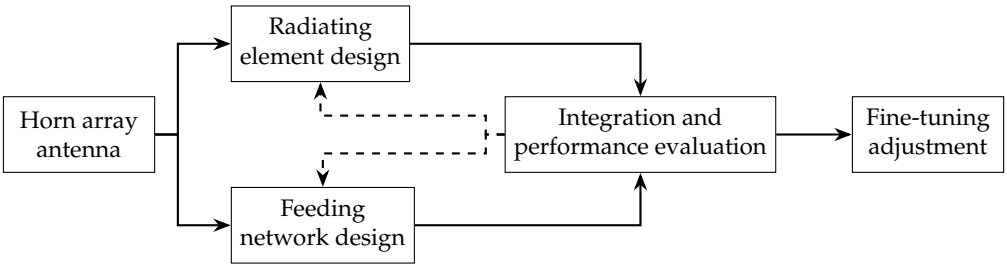


Figure 1. A flowchart of the difference pattern horn array antenna design process.

Translating this methodology to the array design itself results in a topology like the one shown in Figure 2. The feeding network consists of multiple *H*-plane waveguide dividers that directly feed the 16-element array, which is composed of square pyramidal horns, forming a square aperture array. The power dividers are 1:4, meaning 1 input and 4 outputs, with a septum included at the input to ensure good impedance matching and to enhance port isolation within the operating frequency range.

The layout of the *H*-plane dividers is structured progressively. Initially, each antenna has a primary *H*-plane power divider with one input and two outputs. These outputs

then connect to additional dividers, creating an intermediate structure with one input and four outputs. Each of these four stacked outputs, in turn, connects to a divider with a 1:4 configuration, reaching the necessary 1:16 power divider to feed from the input port to the radiating elements.

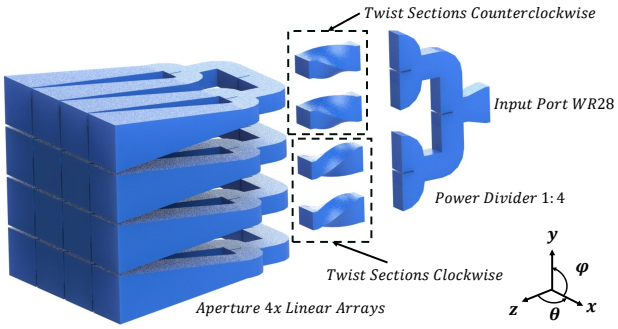
This feed configuration is not unique, as four *E*-plane waveguide dividers (perpendicular to the *z*-axis; see Figure 2) could be used instead to directly reach each of the 16 array inputs. However, using an *H*-plane divider allows for replication in both the vertical and horizontal parts of the network, reducing the overall design complexity.

To connect the primary *H*-plane input divider of the feeding network to each of the four stacked dividers that feed the array, the ports need reorientation. Note that the output ports of the vertical divider are rotated 90 degrees relative to the input ports of the horizontal network dividers; that is, the *E*-plane of the primary divider output corresponds to the *H*-plane of the feeding network inputs. This misalignment is corrected by using a 90° twisted waveguide section. Each twist segment is defined by its length and the 90° rotation angle. Although these elements would not be necessary if using an *E*-plane divider, the addition of the twisted waveguides not only enables the use of a single *H*-plane design but also is responsible for generating a difference pattern.

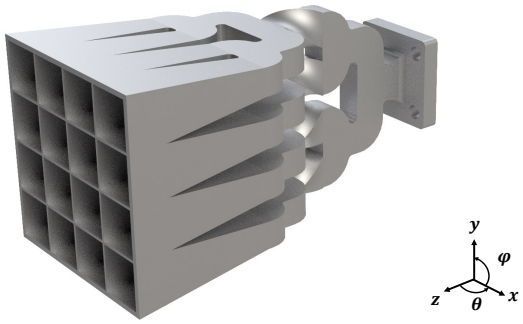
As shown in Figure 2, the twist segments are not identical: the top two twist segments rotate clockwise, while the bottom two rotate counterclockwise. This alternating configuration of twist segments in pairs allows the array's total aperture to be divided into two sub-apertures with respect to the *H*-plane, providing identical amplitude excitation across elements in each sub-aperture but with a 180-degree phase difference. Consequently, a difference pattern is generated. Although this configuration is intricate, it was selected based on its compatibility with the chosen manufacturing process, the details of which will be subsequently explained. Further optimization of the twisted sections' lengths ensures smooth transitions between dividers without impacting impedance matching or degrading the antenna's radiation performance. Adding these twist segments has a minimal effect on the antenna's overall length, but they allow a simplified feeding network by enabling the reuse of identical H-plane dividers across the entire network. Furthermore, Figure 2 shows an exploded view of the difference pattern horn array antenna, featuring two twist sections in the clockwise orientation and two in the counterclockwise orientation from the reference point of the antenna's aperture.

The array is engineered for operation within the 34 to 36 GHz range, aligning with mmWave application requirements. As an initial design choice, a standard WR28 waveguide is considered. However, the spacing of the array elements has been optimized to reduce both the antenna's total dimensions and its weight. This is achieved by implementing a tapered modification to the input waveguide, adjusting its dimensions progressively along the length of the antenna. These tapered changes are visible at the antenna input in the overall views in Figure 2. The WR28 waveguide's standard dimensions are 7.112 mm in height and 3.556 mm in width, while the tapered waveguide ultimately measures 5 mm in height and maintains a width of 3.556 mm, producing a taper specifically in the *H*-plane. A more detailed design process is reported in [33].

The antenna's input design remains compatible with the WR28 rectangular waveguide standard, allowing easy integration with standard transitions. From the antenna's input port, the waveguide width is progressively reduced to align with the width of the *H*-plane power dividers and the horn antenna inputs. It is noteworthy that the electric field at the input is oriented parallel to the *x*-axis.



(**a**)



(**b**)

Figure 2. The difference pattern horn array antenna: (**a**) an exploded view of the vacuum design and (**b**) a rendering of the mechanical design.

For the mechanical design of the differential pattern horn array, once again, thanks to the manufacturing possibilities, an envelope conforming to the vacuum design was created. This envelope typically has a thickness of 1.5 mm while adding extra thickness in the critical areas, i.e., those that could be affected by thermal deformation during manufacturing. Finally, for measuring purposes, the standard WR28 flange was added. Overall, the total length of the difference pattern horn array antenna is 80 mm with an aperture of $41.5 \times 41.5\,\text{mm}^2$.

3. Manufacturing

To validate the design of the proposed horn array difference pattern antenna, incorporating various components such as waveguides, power dividers, twisters, and horn antennas, a decision was made to manufacture and test a monolithic version. AM LPBF was the technology employed for fabrication. This technology involves the deposition of metallic powder layers, around 30 µm, on a building plate, followed by selective melting using a laser beam as a heat source to achieve the desired structure. This procedure is repeated for the different layers until the final part is manufactured. It is worth mentioning that it is not possible to manufacture the design with any subtractive technique in a monolithic piece.

The resulting monolithic piece integrates the horn antenna array with the feeding network, utilizing solely aluminum alloy AlSi10Mg with an electrical conductivity of $\sigma = 1.68 \times 10^7$ S/m [34]. The main advantage of using this method is that it eliminates the need for subsequent assembly and coating steps, streamlining production from two or three steps to just one, thereby reducing potential errors and enhancing device performance. The complexity of the design, including twisted sections, is challenging to produce even in multiple parts via traditional methods, particularly in terms of a difference pattern antenna, where the phase distribution along the aperture of the component is a critical aspect. Since LPBF was chosen from the outset, the antenna design was tailored to accommodate

process constraints. For instance, mechanical surfaces in the 4 × 4 horn antenna array were designed with no inclination exceeding 45° to align with manufacturing capabilities. Additionally, managing high temperatures during production is critical to prevent thermal deformations that could impact the electromagnetic response. Thermal optimization was employed during cooling using multiple thicknesses to mitigate potential deformations.

After manufacturing the monolithic piece using aluminum alloy AlSi10Mg, post-processing steps were initiated. Initially, the piece was detached from the printing bed along with the manufacturing supports. Subsequently, the supports were removed, and the piece underwent thorough cleaning. To further refine the surface, sandblasting was performed using glass microspheres. Finally, a machining cut was applied to the flange area, where an additional thickness of 500 µm had been incorporated to ensure proper contact with the measuring equipment. Overall, a surface roughness of 5–6 µm as-built is expected, and it is reduced to 3–4 µm after sandblasting. Figure 3 depicts photographs of the additively manufactured difference pattern horn array antenna in aluminum alloy AlSi10Mg. The overall size of the array is 41.5 × 41.5 mm^2, with a weight of 52.3 gr.



Figure 3. Photographs of the additively manufactured difference pattern horn array antenna in AlSi10Mg.

4. Experimental Validation

The prototype of the difference pattern horn array antenna, manufactured using additive techniques, underwent measurement and experimental validation at the University of Oviedo, Spain. Initially, scattering parameters were assessed using the Agilent N5247A PNA-X vector analyzer to ensure proper functionality. The reflection coefficient comparison with CST Microwave Studio [35] is depicted in Figure 4. The maximum measured reflection coefficient is −10.8 dB. Despite minor variations, primarily due to manufacturing tolerances, i.e., ±50 µm, the measured results below −10 dB closely align with simulated data, validating the performance of the device.

Once the reflection coefficient was successfully validated, radiation pattern measurements were carried out. Firstly, the prototype of the difference pattern horn array was placed in the anechoic chamber (spherical range) of the University of Oviedo, Spain. In Figure 5a, an image of the measurement setup for the anechoic chamber is depicted. The normalized radiation patterns for the main planes ($\phi = 0°$ and $\phi = 90°$) at 36 GHz are illustrated in Figure 6 for both copolar (CO) and crosspolar (CX) Linear Polarized (LP) field components. In addition, values from a full-wave numerical simulation are compared with measurements, with dashed lines for $\phi = 0°$, dotted lines for $\phi = 90°$, and solid lines for simulations.

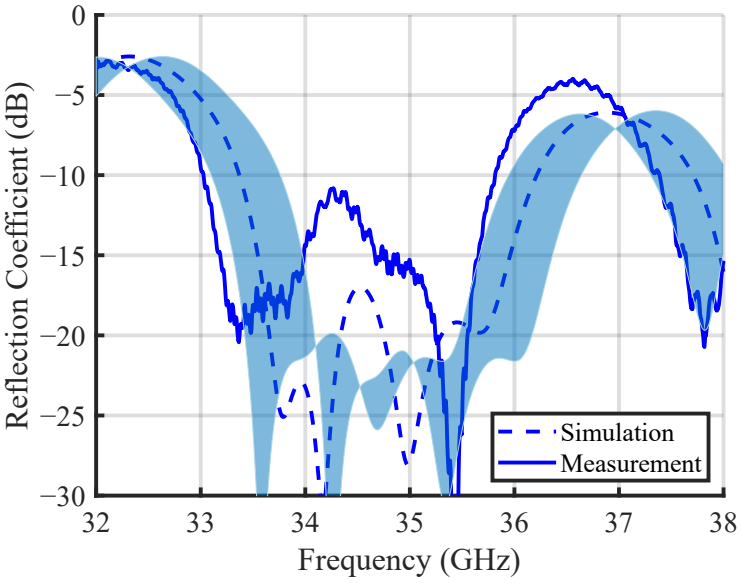
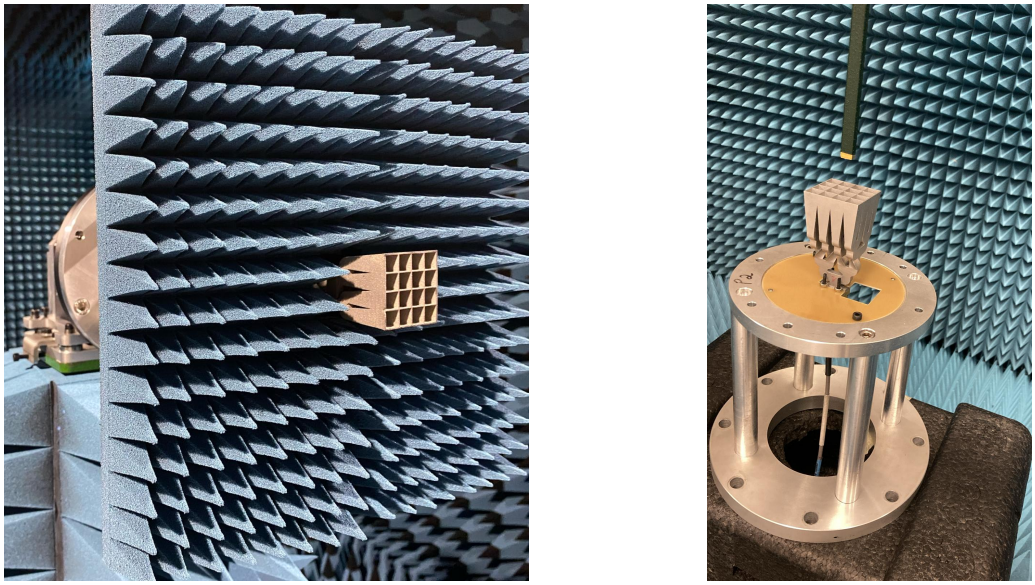


Figure 4. Scattering parameters of difference pattern horn array prototype, comparing measured (*solid lines*) with simulated (*dashed lines*) results with ±1% deviation in shadow.



(**a**) (**b**)

Figure 5. The measurement setup for the additively manufactured horn array prototype in (**a**) the spherical range in an anechoic chamber and (**b**) the planar acquisition range.

Figure 7 displays the measured normalized radiation pattern for CO in the U-V plane at 34, 35, and 36 GHz compared with simulations. Additionally, the results show that the measured level for the null of the copolarized component with respect to the maximum is −27 dB at 36 GHz, with SLLs remaining below −10 dB. More importantly, the level in the null of the radiation pattern was accurately measured for different frequencies. Figure 8 presents the measured level in the center of the radiation pattern from 32 to 36 GHz compared with the simulated value. It is important to note the frequency squint that happens around the center of the pattern due to electrical dimensions. A minimum value of −48.4 dB is measured at 33 GHz.

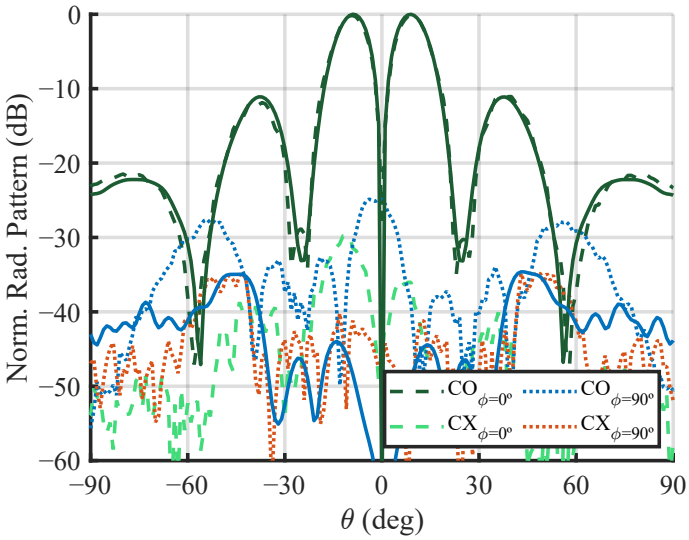


Figure 6. Normalized radiation pattern of difference pattern horn array prototype at 36 GHz, comparing measured (*dashed and dotted lines*) with simulated (*solid lines*) results.

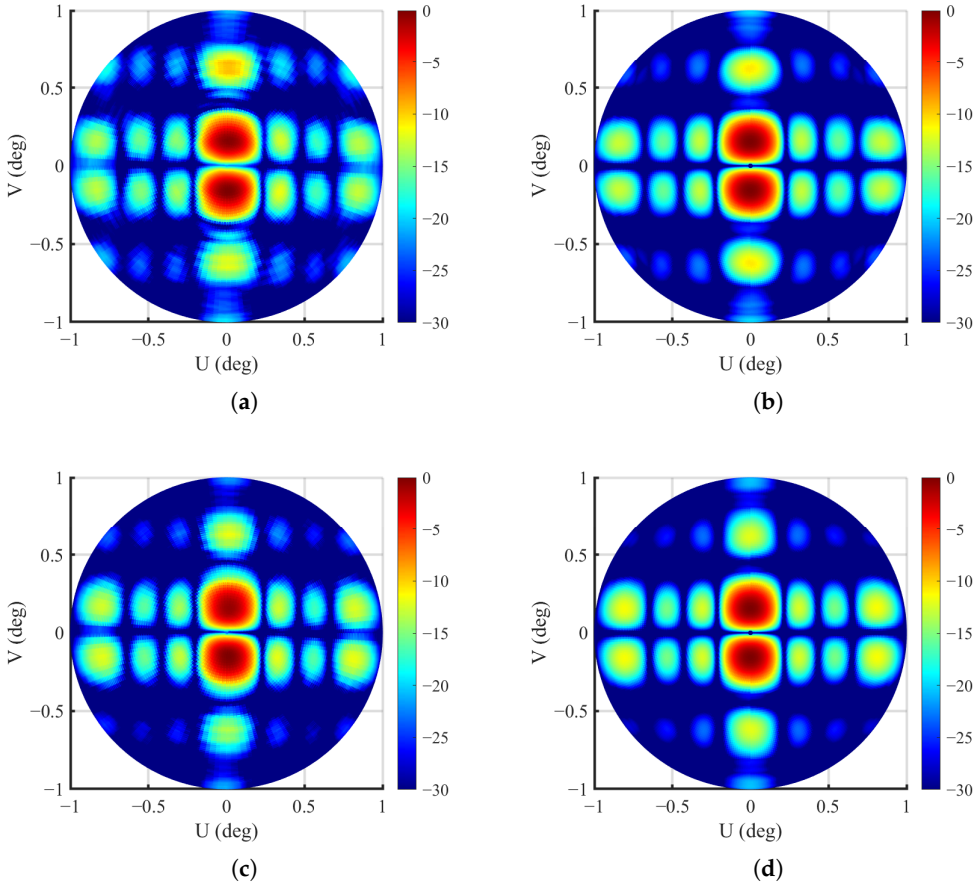


Figure 7. *Cont.*

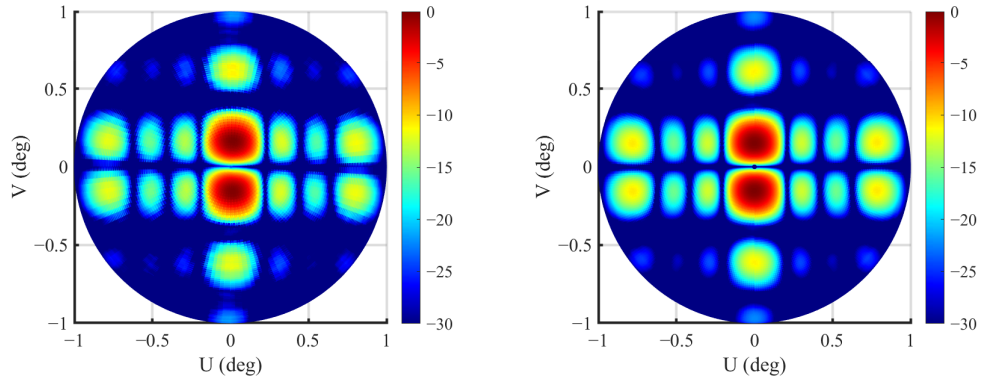


Figure 7. Normalized radiation patterns of the difference pattern horn array in the UV plane for measurements at (**a**) 34 GHz, (**c**) 35 GHz, and (**e**) 36 GHz and simulations at (**b**) 34 GHz (**d**) 35 GHz, and (**f**) 36 GHz.

Furthermore, the prototype was also measured in the planar acquisition range at the University of Oviedo, Spain. The picture in Figure 5b illustrates the prototype of the difference pattern horn array antenna mounted in the measurement setup in a planar acquisition range in a semianechoic environment. The setup comprises an open-ended waveguide in the Ka-band, used as a near-field probe. Both the probe and the prototype are connected to an Agilent N5247A PNA-X vector analyzer. Then, a $100 \times 100\,\text{mm}^2$ plane is measured at 95 mm from the center of the antenna to obtain most of the radiated power. The grid is sampled every mm from 32 to 38 GHz. This measurement campaign is used to evaluate the phase difference in the aperture.

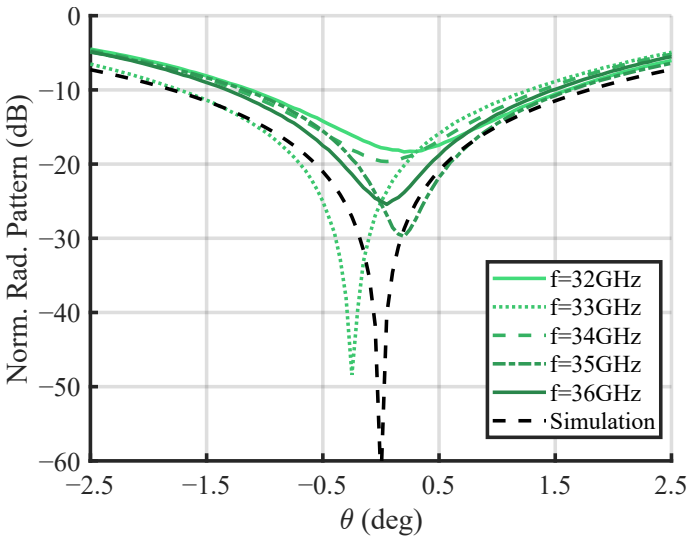


Figure 8. Magnified normalized radiation pattern (cut ϕ = 90°) of difference pattern horn array prototype for different frequencies.

In Figure 9, near-field measurements are illustrated, both in amplitude and in phase, for frequencies of 34, 35, and 36 GHz. Remarkably, in Figure 9a,c,e, amplitudes are shown with a null in the central part for the cut $x = 0$, corresponding to the center of the aperture. Furthermore, in Figure 9b,d,f, it is clearly observed that the upper part of the aperture, i.e., the linear arrays with counterclockwise twists, exhibit a phase difference of 180° compared to the lower part of the aperture, corresponding to the sections with clockwise twists, confirming the correct design and operation of the difference pattern.

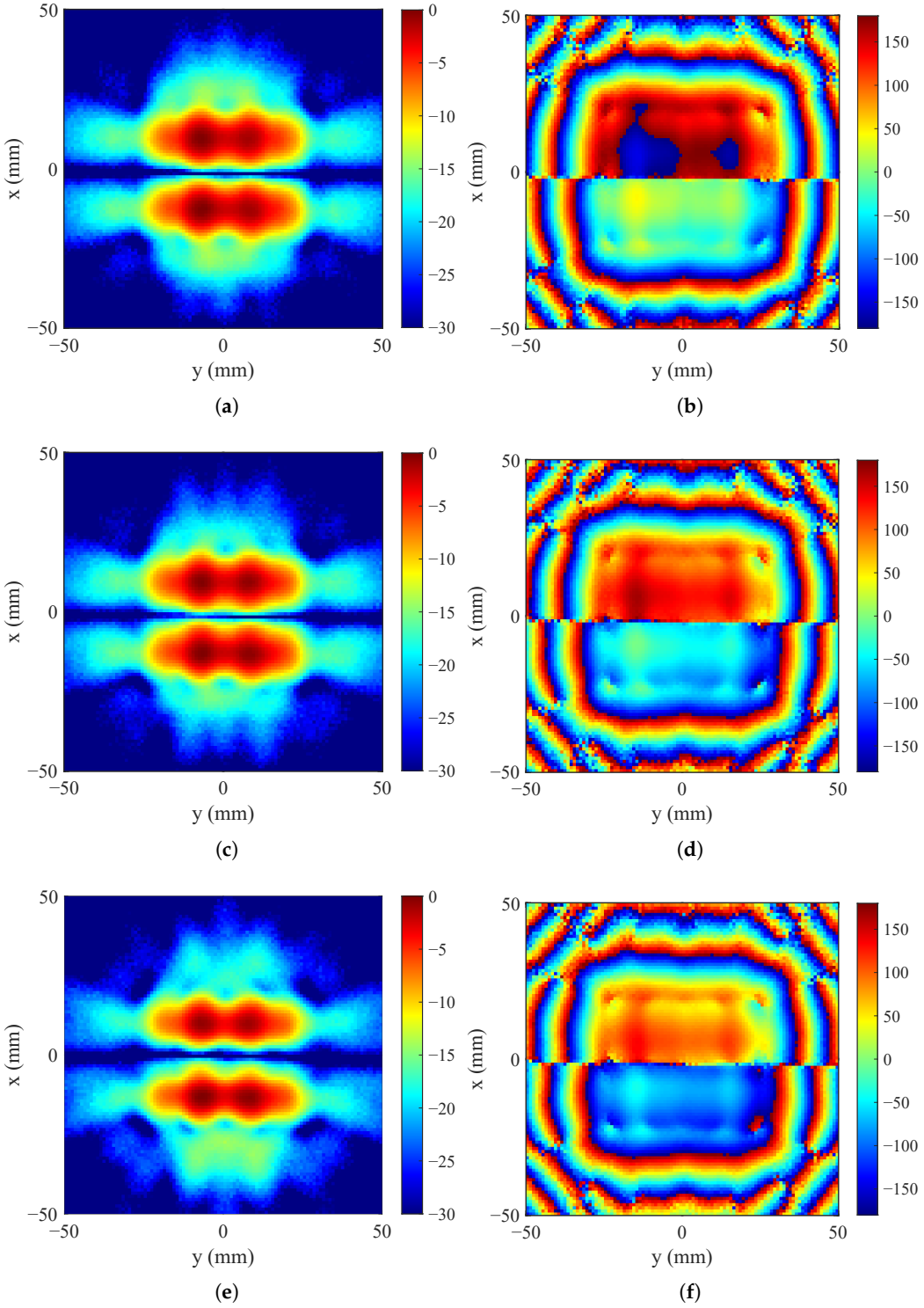


Figure 9. Near-field measurements at 57 mm of difference pattern horn array prototype: (**a**) amplitude and (**b**) phase at 34 GHz, (**c**) amplitude and (**d**) phase at 35 GHz, and (**e**) amplitude and (**f**) phase at 36 GHz.

5. Future Research Lines and Applications

This study demonstrates the potential of AM for designing and producing high-performance monopulse antennas with complex internal geometries, especially in the mm-Wave band. By applying AM techniques, particularly LPBF, to the development of antenna systems, a range of new research directions and applications can be pursued. This

section outlines potential areas for future exploration and improvement, focusing on the capability of AM to facilitate complex waveguide-based designs, produce high-precision difference patterns for monopulse applications, and create scalable, modular antenna arrays suitable for advanced applications.

5.1. Complex Structure Fabrication Using AM

AM offers unique advantages for the construction of intricate geometries that are challenging to achieve with conventional subtractive techniques such as CNC milling. In high-frequency applications, precise geometrical configurations are critical for achieving optimal performance. The LPBF technique used in this study provides a streamlined process for creating these complex structures in a single, monolithic piece, which directly addresses limitations encountered in other conventional methods. Components such as the twisted waveguide sections, which play a crucial role in phase-shifting, or the septum, which enhances impedance matching within the array, are practically unfeasible to monolithically produce through standard machining due to their curved and rotated surfaces with a compact form factor.

By allowing for fully monolithic fabrication, AM removes the need for joint assemblies, which in turn minimizes potential signal losses at connection points, ensures superior structural integrity, and enhances the robustness of the antenna. Future research could explore optimizing new RF devices to integrate into the feeding network, such as filters or OMT, to operate at different frequency bands or dual polarization. In addition, AM facilitates the fabrication of antennas with graded geometries and variable material properties, enabling novel designs that combine mechanical robustness with minimized weight, particularly beneficial for aerospace and satellite applications.

5.2. Enhanced Monopulse Arrays for Difference Pattern Applications

The difference radiation pattern produced by this array design is critical in applications requiring high-precision directional control. Monopulse antennas are used extensively in radar systems for real-time target tracking, in MIMO communication systems for optimized signal reception, and in radio astronomy for capturing celestial signals with high directional accuracy. The flexibility provided by AM allows for intricate designs that can integrate advanced monopulse features, such as fine-tuned phase and amplitude differences across array elements. These features contribute to improved beam-steering and direction-finding capabilities, which are especially valuable in target-tracking applications and satellite communications.

Future research could expand on the current design by incorporating adaptive tuning elements or multi-band capabilities, allowing a single array structure to operate effectively across multiple frequency bands or in reconfigurable scenarios. This would further exploit AM's ability to handle complex internal designs that integrate electronic components or embedded waveguides, enhancing the antenna capability to different communication standards.

5.3. Scalable and Modular Array Design

The 16-element array presented in this work serves as a foundational module that can be scaled to accommodate larger arrays, addressing the need for high-gain, high-resolution antenna systems. Modular scaling of the array is feasible due to the precision and repeatability offered by AM, which enable the creation of identical, easily integrated units. This modular approach simplifies the assembly of larger arrays without the need for additional alignment or calibration, which would typically introduce phase errors and degrade overall performance. By designing each array segment as a self-contained module with its own feeding network, larger arrays can be assembled to meet the needs of high-resolution radar or long-range communication systems.

In future designs, this modular approach could allow for the stacking or interlocking of multiple array units, enabling flexible configuration and incremental performance

upgrades. Such scalable configurations are highly desirable in radar and remote sensing, where resolution is critical. AM can support this modular architecture by maintaining the necessary accuracy across a large number of identical components, ensuring that the performance characteristics of each module remain consistent throughout the array.

6. Conclusions

In this work, a fully metallic horn array antenna with a difference pattern was designed and validated for operation in the K_a-band, showcasing the potential of additive manufacturing (AM), specifically Laser Powder-Bed Fusion (LPBF), in producing high-precision, monolithic microwave components. The monolithic nature of the design allows for the integration of *H*-plane power dividers and complex 90° twist sections, which are otherwise challenging to manufacture with conventional methods. This approach minimizes alignment errors and leakage, yielding robust and compact structures that are well suited for high-performance mm-Wave applications. The prototype, additively manufactured and measured in both a far-field spherical range and planar near-field scanner, demonstrated stable performance across the operating bandwidth, achieving a -48.4 dB null at 33 GHz in the difference pattern, with minimal frequency squinting.

Overall, this study illustrates how AM not only addresses longstanding manufacturing limitations in high-frequency antenna designs but also opens new pathways for innovation in antenna systems with complex geometries and modular configurations. This work shows how LPBF allows not only the design but also the fabrication of antenna geometries that, until now, could not be realized due to the limitations of conventional manufacturing processes. In particular, it presents a design that integrates a 16×16-element array with a feeding network containing complex elements, such as 90-degree twisted sections. Additionally, a difference diagram is presented, which is very sensitive to design and manufacturing errors, as the array elements must be fed properly, not only in amplitude but also in achieving out-of-phase feeding, which is highly sensitive. Therefore, this work not only presents the design of an RF component but also addresses the design and testing of a monolithic device with high-sensitivity performance, presenting a system-level design. The successful application of LPBF in this project affirms AM's suitability for developing scalable difference pattern arrays and modular arrays optimized for mm-Wave applications, underscoring its significance in advancing the next generation of high-frequency antenna systems.

Author Contributions: Conceptualization, M.A. and Á.F.V.; Analysis and Design, J.R.-F. and Á.F.V.; Simulation Analysis, J.R.-F., Á.F.V., M.R.P. and M.A.; Manufacturing, J.R.-F.; Measurements, M.R.P.; Draft Preparation, J.R.-F.; Writing–Review, Á.F.V., M.R.P. and M.A.; Supervision, M.R.P. and M.A.; Funding Acquisition, M.A. All authors have read and agreed to the published version of the manuscript.

Funding: This work was supported in part by MCIN/AEI/10.13039/501100011033 under grants PID2020-114172RB-C21, PID2023-146246OB-C32, and TED2021-130650B-C22, cofunded by the EU's (European Union) "NextGenerationEU"/PRTR and by the Spanish Ministry of Universities and European Union (NextGenerationEU fund) under grant MU-21-UP2021-03071895621J.

Institutional Review Board Statement: Not applicable.

Informed Consent Statement: Not applicable.

Data Availability Statement: The raw data supporting the conclusions of this article will be made available by the authors on request.

Conflicts of Interest: Author José Rico-Fernández was employed by the company Northern Waves AB. The remaining authors declare that the re-search was conducted in the absence of any commercial or financial relationships that could be construed as a potential conflict of interest.

References

1. Peverini, O.A.; Lumia, M.; Addamo, G.; Virone, G.; Fonseca, N.J.G. How 3D-Printing Is Changing RF Front-End Design for Space Applications. *IEEE J. Microw.* **2023**, *3*, 800–814. [CrossRef]
2. Zhang, S.; Arya, R.K.; Whittow, W.G.; Cadman, D.; Mittra, R.; Vardaxoglou, J.C. Ultra-Wideband Flat Metamaterial GRIN Lenses Assisted With Additive Manufacturing Technique. *IEEE Trans. Antennas Propag.* **2021**, *69*, 3788–3799. [CrossRef]
3. Poyanco, J.M.; Pizarro, F.; Rajo-Iglesias, E. 3D-printed Integrated GRIN Lens-Polarizer Using Anisotropic Materials. *IEEE Trans. Antennas Propag.* **2024**, *72*, 5343–5348. [CrossRef]
4. Melendro-Jimenez, J.; Sanchez-Olivares, P.; Tamayo-Dominguez, A.; Sun, X.; Fernandez-Gonzalez, J.M. 3D Printed Directive Beam-Steering Antenna Based on Gradient Index Flat Lens with an Integrated Polarizer for Dual Circular Polarization at W-Band. *IEEE Trans. Antennas Propag.* **2023**, *71*, 1059–1064. [CrossRef]
5. Zetterstrom, O.; Fonseca, N.J.G.; Quevedo-Teruel, O. Compact Half-Luneburg Lens Antenna Based on a Glide-Symmetric Dielectric Structure. *IEEE Antennas Wirel. Propag. Lett.* **2022**, *21*, 2283–2287. [CrossRef]
6. Massaccesi, A.; Pirinoli, P.; Bertana, V.; Scordo, G.; Marasso, S.L.; Cocuzza, M.; Dassano, G. 3D-Printable Dielectric Transmitarray with Enhanced Bandwidth at Millimeter-Waves. *IEEE Access* **2018**, *6*, 46407–46418. [CrossRef]
7. Matos, S.A.; Teixeira, J.P.; Costa, J.R.; Fernandes, C.A.; Nachabe, N.; Luxey, C.; Titz, D.; Gianesello, F.; del Rio, C.; Arboleya, A.; et al. 3-D-Printed Transmit-Array Antenna for Broadband Backhaul 5G Links at V-Band. *IEEE Antennas Wirel. Propag. Lett.* **2020**, *19*, 977–981. [CrossRef]
8. Vaquero, A.F.; Teixeira, J.; Matos, S.A.; Arrebola, M.; Costa, J.R.; Felicio, J.M.; Fernandes, C.A.; Fonseca, N.J.G. Design of Low-Profile Transmitarray Antennas With Wide Mechanical Beam Steering at Millimeter Waves. *IEEE Trans. Antennas Propag.* **2023**, *71*, 3713–3718. [CrossRef]
9. Rebollo, A.; Vaquero, A.F.; Arrebola, M.; Pino, M.R. 3D-Printed Dual-Reflector Antenna With Self-Supported Dielectric Subreflector. *IEEE Access* **2020**, *8*, 209091–209100. [CrossRef]
10. Vaquero, A.F.; Rebollo, A.; Arrebola, M. Additive manufacturing in compact high-gain wideband antennas operating in mm-wave frequencies. *Sci. Rep.* **2023**, *13*, 10998. [CrossRef]
11. Dorlé, A.; Gillard, R.; Menargues, E.; Van Der Vorst, M.; De Rijk, E.; Martín-Iglesias, P.; García-Vigueras, M. Additive Manufacturing of Modulated Triple-Ridge Leaky-Wave Antenna. *IEEE Antennas Wirel. Propag. Lett.* **2018**, *17*, 2123–2127. [CrossRef]
12. Tamayo-Domínguez, A.; Fernández-González, J.M.; Sierra-Castañer, M. 3-D-Printed Modified Butler Matrix Based on Gap Waveguide at W-Band for Monopulse Radar. *IEEE Trans. Microw. Theory Tech.* **2020**, *68*, 926–938. [CrossRef]
13. Tamayo-Dominguez, A.; Sanchez-Olivares, P.; Camacho-Hernandez, A.; Fernandez-Gonzalez, J.M. Guidelines for Accurate in-House Electroplating and 3-D-Printing Processes Applied to mm-Wave Devices. *IEEE Microw. Wirel. Compon. Lett.* **2022**, *32*, 1267–1270. [CrossRef]
14. Skaik, T.; Salek, M.; Hunyor, P.; Wang, H.; Huggard, P.G.; Wilson, P.F.; Williams, M.A.; Wang, Y. Evaluation of 3D Printed Monolithic G-band Waveguide Components. *IEEE Trans. Compon. Packaging Manuf. Technol.* **2023**, *13*, 240–248. [CrossRef]
15. Santiago, D.; Laso, M.A.G.; Lopetegi, T.; Arregui, I. Novel Design Method for Millimeter-Wave Gap Waveguide Low-Pass Filters Using Advanced Manufacturing Techniques. *IEEE Access* **2023**, *11*, 89711–89719. [CrossRef]
16. Addamo, G.; Vigolo, M.C.; Virone, G.; Peverini, O.A.; Bozzi, M.; Perregrini, L. Additive Manufacturing of Ka-Band Dual-Polarization Waveguide Components. *IEEE Trans. Microw. Theory Tech.* **2018**, *66*, 3589–3596. [CrossRef]
17. González-Calvo, M.; Montejo-Garai, J.R.; Ruiz-Cruz, J.A.; Rebollar, J.M. Additive Manufacturing of a High-Performance Q-Band Circular TE01 Mode Flared-Type Transducer. *IEEE Microw. Wirel. Compon. Lett.* **2019**, *29*, 577–579. [CrossRef]
18. Salazar, R.; Pizarro, F.; Vasquez, D.; Rajo-Iglesias, E. Assessment of 3D-printed Waveguides Using Conductive Filaments and a Chloroform-based Smoothing Process. *Addit. Manuf.* **2022**, *51*, 102593. [CrossRef]
19. Beccaria, M.; Addamo, G.; Orefice, M.; Peverini, O.; Manfredi, D.; Calignano, F.; Virone, G.; Pirinoli, P. Enhanced Efficiency and Reduced Side Lobe Level Convex Conformal Reflectarray. *Appl. Sci.* **2021**, *11*, 9893. [CrossRef]
20. Castillo-Tapia, P.; Rico-Fernández, J.; Quevedo-Teruel, O. V-Band Monolithic Additive-Manufactured Geodesic Lens Array Antenna. *IEEE Antennas Wirel. Propag. Lett.* **2023**, *22*, 2527–2531. [CrossRef]
21. Castillo-Tapia, P.; Rico-Fernández, J.; Clendinning, S.; Mesa, F.; Quevedo-Teruel, O. Evaluation of Losses in 3D-Printed Geodesic Lenses Using a Ray-Tracing Model. *IEEE Trans. Antennas Propag.* 2023, *in press*.
22. Fonseca, N.J.G.; Gomanne, S.A.; Rico-Fernández, J.; Jankovic, P.; Galdeano, J.; Toso, G.; Angeletti, P.; Arrebola, M.; Quevedo-Teruel, O. Fully-Metallic Additively Manufactured Monolithic Double-Ridged Waveguide Rotman Lens in the K/Ka-Band. *Sensors* **2023**, *23*, 6573. [CrossRef] [PubMed]
23. Rico-Fernández, J.; Vidarsson, F.V.; Arrebola, M.; Fonseca, N.J.; Quevedo-Teruel, O. Compact and Lightweight Additive Manufactured Parallel-Plate Waveguide Half-Luneburg Geodesic Lens Multiple-Beam Antenna in the K_a-Band. *IEEE Antennas Wirel. Propag. Lett.* **2023**, *22*, 684–688. [CrossRef]
24. Gini, F.; Bordoni, F.; Farina, A. Multiple radar targets detection by exploiting induced amplitude modulation. *IEEE Trans. Signal Process.* **2004**, *52*, 903–913. [CrossRef]
25. Li, H.; Lau, B.K.; He, S. Design of Closely Packed Pattern Reconfigurable Antenna Array for MIMO Terminals. *IEEE Trans. Antennas Propag.* **2017**, *65*, 4891–4896. [CrossRef]
26. Kardashev, N.S. An omnidirectional search for monopulse signals from astronomical objects. *Sov. Astron.* **1977**, *21*, 1–9.
27. Skolnik, M. *Radar Handbook*, 2nd ed.; McGraw-Hill: New York, NY, USA, 1990.

28. Sherman, S.; Barton, D. *Monopulse Principles and Techniques*; Artech House Radar Library, Artech House: New York, NY, USA, 2011.
29. Tekkouk, K.; Ettorre, M.; Le Coq, L.; Sauleau, R. SIW Pillbox Antenna for Monopulse Radar Applications. *IEEE Trans. Antennas Propag.* **2015**, *63*, 3918–3927. [CrossRef]
30. Liu, B.; Hong, W.; Kuai, Z.; Yin, X.; Luo, G.; Chen, J.; Tang, H.; Wu, K. Substrate Integrated Waveguide (SIW) Monopulse Slot Antenna Array. *IEEE Trans. Antennas Propag.* **2009**, *57*, 275–279. [CrossRef]
31. Cheng, Y.J.; Hong, W.; Wu, K. 94 GHz Substrate Integrated Monopulse Antenna Array. *IEEE Trans. Antennas Propag.* **2012**, *60*, 121–129. [CrossRef]
32. Faenzi, M.; González-Ovejero, D.; Petraglia, G.; D'Alterio, G.; Pascariello, F.; Vitiello, R.; Maci, S. A Metasurface Radar Monopulse Antenna. *IEEE Trans Antennas Propag.* **2022**, *70*, 2571–2579. [CrossRef]
33. Alonso-González, L.; Rico-Fernández, J.; Vaquero, A.F.; Arrebola, M. Metal-Only Additive-Manufactured in Monolithic Piece Array for Sum/Difference Pattern in Ka-Band. *IEEE Trans. Antennas Propag.* **2023**, *71*, 6413–6422. [CrossRef]
34. Silbernagel, C.; Ashcroft, I.; Dickens, P.; Galea, M. Electrical resistivity of additively manufactured AlSi10Mg for use in electric motors. *Addit. Manuf.* **2018**, *21*, 395–403. [CrossRef]
35. SIMULIA, Johnston, RI, USA, Dassault Systemes Deutschland GmbH: Waltham, MA, USA. CST Studio Suite 2023. Available online: http://cst.com/ (accessed on 23 November 2024).

Disclaimer/Publisher's Note: The statements, opinions and data contained in all publications are solely those of the individual author(s) and contributor(s) and not of MDPI and/or the editor(s). MDPI and/or the editor(s) disclaim responsibility for any injury to people or property resulting from any ideas, methods, instructions or products referred to in the content.